NILU Norsk institutt for luftforskning
Norwegian Institute for Air Research

OR 39/2013

Measurement of volcanic ash in Norwegian air space

WP 1.4.2 Improved detection of ash clouds

Arve Kylling

Scientific report

WP 1.4.2 Improved detection of ash clouds

Arve Kylling
NILU-Norwegian Institute for Air Research
Kjeller, Norway

October 14, 2013

Contents

1 Introduction

A number of satellite instruments have been used to detect volcanic ash (see Thomas and Watson, 2010, for a recent overview). For Norwegian and surrounding air space, the Spinning Enhanced Visible and Infrared Imager (SEVIRI) provides high temporal and spatial coverage. Due to its geostationary orbit, the spatial resolution detoriates from 3×3 km^2 at the equator to about 5×5 to 10×10 km^2 for Norwegian latitudes (Fig. 1 Prata and Prata, 2012). The time resolution is normally 15 min, but this may be decreased to 5 min in the "rapid scan" mode[1]. Eight of SEVIRI's twelve channels are in the infrared (IR). Contrary to the solar channels, the IR channels provide 24 hours coverage. Thus, due to the high temporal and spatial resolution, and the geographical coverage, this report will focus on the detection of volcanic ash using the IR channels of the SEVIRI instrument.

First a brief descripton of the SEVIRI IR-channels. This is followed by a summary of various ash detection methods applicable to the SEVIRI instrument. A subset of the methods are compared using a synthetic data set.

2 The IR channels of the SEVIRI instrument

The main characteristcs of the SEVIRI IR channels are briefly summarized in Table 1. For detection of clouds the

Table 1: Summary of the SEVIRI IR channels. Further information is available from http://oiswww.eumetsat.org/WEBOPS/msg_interpretation/msg_channels.php.

Channel (μm)	Comments
3.9	Window channel close to CO_2 band, affected by solar radiation during day time. Detection of low cloud and fog and thin cirrus.
6.2	Water vapour absorbs around 6 μm. Channel in band center. Sees higher atmospheric levels.
7.3	Water vapour absorbs around 6 μm. Channel in band wing. Sees lower atmospheric levels as well.
8.7	SO_2 absorption, window channel, cloud systems
9.7	Covers ozone absorption band.
10.8	Window channel, cloud systems
12.0	Window channel, cloud systems
13.4	Covers CO_2 absorption band.

window channels are preferred. For 24 hour surveillance with a single method the 3.9 μm has limitations as it is influenced by solar radiation. Furthermore, the 6.2 and 7.3 μm channels are of limited use due to the absorption band of water vapour around 6 μm. The remaining channels may be used to identify clouds. The various types of clouds, ice and liquid water clouds and ash clouds, have different optical properties. The variations of the optical properties with wavelength may be used to discriminate ash clouds from meteorological clouds. In Fig. 1

is shown the wavelength dependence of the emissivity of some model ice, liquid water and volcanic ash clouds. Of special interest is the different behaviour of ash and liquid and ice water clouds between 11 and 13 μm. The emissivity of the ash cloud is seen to decrease while the emissivity of liquid water and ice clouds increase in this wavelength region. Hence, for ice and water clouds the brightness temperature, BT, in the 10.8 μm channel is larger than in the 12.0 μm channel[2]. That is $BT_{11} > BT_{12}$ and $dBT = BT_{11} - BT_{12} > 0$. For ash clouds $dBT = BT_{11} - BT_{12} < 0$. Thus, the brightness temperature difference between the 10.8 and 12.0 μm channels may be used to discriminate between meteorological clouds and volcanic ash clouds. This method to identify ash clouds was introduced by Prata (1989) and is often referred to as the 'reverse absorption' technique. Variants of this method have later been developed. They are described in the next section.

[1] For more information about rapid scanning see http://www.eumetsat.int/website/home/Satellites/CurrentSatellites/Meteosat/RapidScanningService/index.html.

[2] See Appendix A for a justification.

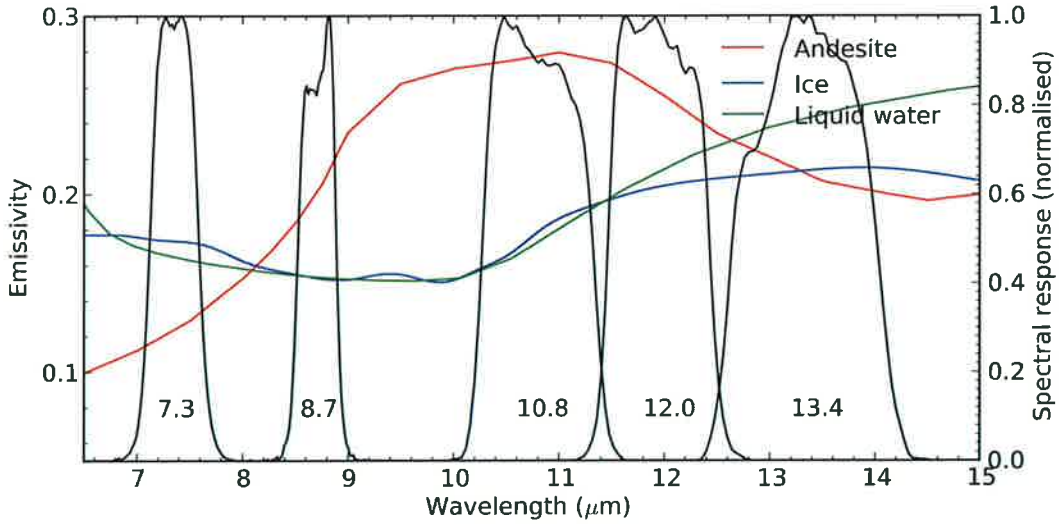

Figure 1: The emissivities of an ice (blue), liquid water (green) and volcanic ash (red) cloud. All clouds are plane-parallel. The ice cloud is located between 10 and 11 km with an ice water content of 0.005 g/m^3 and contains spherical ice particles with an effective radius of 20 μm. The water cloud extends from 2 to 5 km, has a liquid water content of 0.001 g/m^3 and water droplets with an effective radius of 10 μm. The ash cloud has a density of 0.002 g/m^2 and is located between 9 and 10 km. The ash particles making up the ash cloud are assumed to have a radius of 3.0 μm. In black is shown the spectral response of various SEVIRI IR channels. Note that the 9.7 μm channel is not shown.

It is noted that dBT is negative for only a limited range of ash particle sizes. Under the assumption that the ash particles are spherical and monodispersed, Wen and Rose (1994) found that negative brightness temperature differences are only present for particle sizes smaller than 5 μm. Often larger effective particle radii are reported for retrieved volcanic ash properties. The effective radius, (r_e), is defined as

$$r_e = \frac{\int \pi r^3 n(r) dr}{\int \pi r^2 n(r) dr}, \tag{1}$$

where $n(r)$ is the number size distribution and r the ash particle radius. Depending on the shape of $n(r)$, the effective radius may be significantly different from the radius of monodipersed particles.

3 Volcanic ash cloud detection methods

Various methods based on the 'reverse absorption' technique described by Prata (1989), have been published over the years. While all methods rely on the different optical properties of ash and meteorological cloud in the IR window channels, they have different approaches for correcting for water vapor absorption and to a certain extent, the mixing of cloud types. Below various ash discrimination methods are described.

3.1 dBT-scheme from Prata and Prata (2012) , the VOLE ash product

The method described by Prata and Prata (2012) is similar to the VOLE ash product from EUMETSAT[3]. It consists basically of the following steps.

[3]For VOLE information see for example http://navigator.eumetsat.int/discovery/Start/DirectSearch/DetailResult.do?f%28r0%29=EO:EUM:DAT:MSG:VOLE.

1. The brightness temperature difference $BT_{10.8} - BT_{12.0}$ is corrected for water vapour absorption as described in Yu et al. (2002). They derived empirical upper and lower bound relations between $BT_{10.8} - BT_{12.0}$ and $BT_{10.8}$ due to the nonlinear relationship between sea surface temperature and precipitable water and thus between $BT_{10.8} - BT_{12.0}$ and $BT_{10.8}$ through precipitable water. To correct for the water vapour correction the lower bound is used:

$$\Delta BT_{wv} = \exp(6T^{\star} - b). \tag{2}$$

Here ΔBT_{wv} is the correction due to the difference in water vapour absorption between 10.8 and 12.0 μm, and is to be subtracted from $BT_{10.8} - BT_{12.0}$. Furthermore, $T^{\star} = BT_{10.8}/BT_{\text{max}}$ where $BT_{\text{max}} = 320$ K (Yu et al., 2002). The parameter b determines the value of the water vapour correction at maximum $BT_{10.8}$ by equating the lower bound, Eq. 2 and the upper bound

$$\Delta BT_{wv} = \exp(20BT^{\star} - 18). \tag{3}$$

giving

$$b = 18 - 14BT_{10.8}^{\text{max}}/BT_{\text{max}} \tag{4}$$

The value of $BT_{10.8}^{\text{max}}$ may either be chosen by searching the scene for the maximum value of $BT_{10.8}$ or by manually selecting a representative for $BT_{10.8}^{\text{max}}$ from the scene. The water vapour correction is defined for nadir view. Hence a simple path correction is applied to the water vapor correction term for slant observation geometries.

2. Pixels are identified as containing ash if

$$BT_{10.8} - BT_{12.0} < \Delta BT_{cut} \tag{5}$$

where $\Delta BT_{cut} = -0.8$ K for the Eyjafjallajökull 2010 eruption.

The above method is simple and powerful, albeit there are also problems as it produces too many false positives. Reasons for this has been given by Prata et al. (2001) and include situations in absence of ash for which

1. Strong temperature inversions near the surface may give negative dBT.
2. Desert type surfaces may give negative dBT.
3. Cloud tops overshooting the tropopause may give negative dBT.
4. Instrument noise or collocation errors between channels may give negative dBT.

Various ways have been devised to overcome these problems and they are included in the methods described below.

3.2 KNMI scheme from de LaaT and van der A De Bilt (2012)

To avoid too many false positives the following ash detection scheme has been developed by researchers from the KNMI - Koninklijk Nederlands Meteorologisch Instituut (de LaaT and van der A De Bilt, 2012). The scheme uses the 8.7, 10.8 and 12.0 μm channels of SEVIRI. A pixel is said to contain ash if the following criteria are satisfied:

$$(BT_{10.8} - BT_{12.0}) < -1.0 \text{ K} \tag{6}$$

AND

$$(BT_{10.8} - BT_{8.7}) < 5.0 \text{ K} \tag{7}$$

AND

$$BT_{10.8} < 300.0 \text{ K} \tag{8}$$

3.3 β-ratio scheme from Pavolonis et al. (2013)

Another approach to detection of ash clouds is the use of β-ratios. The β-ratio is defined as (Eq. 3, Pavolonis (2010))

$$\beta(\lambda_1, \lambda_2) = \frac{\ln[1 - \epsilon(\lambda_1)]}{\ln[1 - \epsilon(\lambda_2)]} = \frac{\tau_{abs,eff}(\lambda_1)}{\tau_{abs,eff}(\lambda_2)} \tag{9}$$

and can be interpreted as the ratio of the effective absorption optical depth at two wavelengths. The β-ratio may be calculated from observations using the following expression for the emissivity (Eq. 2 Pavolonis, 2010)

$$\epsilon(\lambda) = \frac{R_{\text{obs}}(\lambda) - R_{\text{clr}}(\lambda)}{[B(\lambda, T_{\text{eff}})T_{\text{ac}}(\lambda) + R_{\text{ac}}(\lambda)] - R_{\text{clr}}(\lambda)}. \tag{10}$$

Here

$R_{\text{obs}}(\lambda)$ is the observed radiance from SEVIRI.

$R_{\text{clr}}(\lambda)$ is the clear sky radiance as calculated be a radiative transfer model.

$R_{\text{ac}}(\lambda)$ The above cloud upwelling atmospheric radiance as calculated be a radiative transfer model.

$T_{\text{ac}}(\lambda)$ The above cloud atmospheric transmittance as calculated be a radiative transfer model.

$B(\lambda, T_{\text{eff}})$ The Planck function at the effective cloud temperature T_{eff}.

Ash pixels are identified by requiring the top of troposphere emissivity at 10.8 μm, $\epsilon_{10.8}$, to be greater than T_{emiss}, where $T_{emiss} = 0.02$ or 0.10, see Fig. 4, Pavolonis et al. (2013). Furthermore, it is required that

$$\beta(12.0/10.8) < 1.0 \quad \text{for} \quad \beta(8.7/10.8) < 1.0 \tag{11}$$

$$\beta(12.0/10.8) = 1.0 \text{ to } 0.85 \quad \text{for} \quad 1.0 < \beta(8.7/10.8) < 1.15 \tag{12}$$

$$\beta(12.0/10.8) < 0.85 \quad \text{for} \quad \beta(8.7/10.8) > 1.15 \tag{13}$$

AND

$$(BT_{10.8}^{obs} - BT_{12.0}^{obs}) - (BT_{10.8}^{clear} - BT_{12.0}^{clear}) < -0.5 \text{ K} \tag{14}$$

Finally, cloud object defined as ash if at least one pixel in cloud object classified as ash, where cloud object is defined as in Wielicki and Welch (1986).

3.4 Scheme from Francis et al. (2012)

Francis et al. (2012) have used data from the Eyjafallajökull 2010 eruption to test their ash detection and retrieval method. It uses a combination of brightness temperature differences and the β-ratio concept. It consists of five steps as follows:

1. Definite ash detection by requiring

$$BT_{10.8} - BT_{12.0} < -2 \text{ K} \tag{15}$$

2. Tenative ash detection flag given to pixels where

$$BT_{10.8} - BT_{12.0} + BT_{10.8} - BT_{8.7} < 1.5 \text{ K} \tag{16}$$

3. Ash detection including water vapour correction. The clear sky brightness temperatures are calculated with the RTTOV radiative transfer model with input from a weather forecast model.

$$BT_{10.8} - BT_{12.0} < 0.7 \text{ K}$$
$$\text{AND} \tag{17}$$
$$BT_{10.8} - BT_{12.0} < BT_{10.8}^{clr} - BT_{12.0}^{clr} - 1.0 \text{ K}$$

4. Removal of false positives using β-ratios.

$$\begin{aligned} &\beta(8.7, 10.8) \leq 0.7 \\ &\qquad \text{OR} \\ &\beta(8.7, 10.8) \geq 1.2 \\ &\qquad \text{OR} \\ &\beta(12.0, 10.8) > a_0 + a_1\beta(8.7, 10.8) + a_2\beta(8.7, 10.8)^2 \end{aligned} \tag{18}$$

where $a_0 = 4.264, a_1 = -5.823, a_2 = 2.446$ and

$$\beta(8.7, 10.8) = \frac{\ln(1 - \epsilon_{8.7})}{\ln(1 - \epsilon_{10.8})} \tag{19}$$

5. Spatial noise-reduction by retaining ash flag on pixel only if at least 6 out of 9 pixels in a 3×3 surrounding pixel box have been flagged.

3.5 VAST Cloud Identification (CID)

As part of the European Space Agency (ESA) funded Volcanic Ash Strategic initiative Team (VAST) project, a new ash detection method has been developed and reported by Prata (2013). The method uses a number of tests to identify false positive ash pixels. The 3.9 (night only), 6.2, 7.3, 8.7, 9.7, 10.8, 12.0 and 13.4 μm channels are utilized. The tests correct for viewing angle, land surface, cloud, and water vapour effects.

1. Reverse absorption, $BT_{10.8} - BT_{12.0} < \Delta BT_{cut}$, where $\Delta BT_{cut} = -0.8$ K.
2. Identification of non-ash clouds, $BT_{13.2} - BT_{9.7} < \Delta BT_2$, where $\Delta BT_2 = 0.0$ K.
3. Viewing angle (θ) dependent dBT, $BT_{10.8} - BT_{12.0} < \Delta BT_1/\cos(\theta)$, where $\Delta BT_1 = -0.2$ K.
4. Non-ash cloud spatial uniformity test, $\sigma(BT_{10.8} - BT_{12.0}) > \sigma_{N_s}$, where $N_s = 5$, and $\sigma_{N_s} = -0.9(-0.3)$K over ocean (land).
5. Land emissivity test, $BT_{10.8\epsilon} - BT_{12.0\epsilon} > \Delta BT_\epsilon + \Delta BT_\epsilon(t)$ and $BT_{10.8} - BT_{12.0} < \Delta BT_{cut}$ and $BT_{12.0} > T_{250}$, where $\Delta BT_\epsilon(t) = -1 + \cos(2\pi t/24)$, $\Delta BT_\epsilon = -0.2$, $\epsilon_{10.8} = 0.988$, $\epsilon_{12.0} = 0.970$ and t is time in hours. $BT_{10.8\epsilon}$ refers to calculated brightness temperature for at emissivity ϵ. ΔBT_{cut} as above.
6. Low uniform cloud over ocean, $BT_{10.8} - BT_{12.0} < \Delta BT_{cut}$ and $BT_{9.7} - BT_{13.2} > T_{240}$, where $T_{240} = 240.0$ K. ΔBT_{cut} as above.
7. Clouds at large viewing angle at night, $BT_{10.8} - BT_{12.0} < \Delta BT_{cut}$ and $BT_{3.9} - BT_{12.0} > \Delta BT_3/\cos(\theta)$, where $\Delta BT_3 = 200.0$ K. ΔBT_{cut} as above.
8. Exclude pixels at large viewing angles, $\theta > \theta_{max}$, where $\theta_{max} = 75°$.
9. Clouds at large viewing angles, $BT_{9.7} - BT_{13.2} + BT_{7.3} - BT_{6.2} < \Delta BT_4$, and $\theta > \theta_0$, where $\Delta BT_4 = 7.0$ K and $\theta_0 = 72°$.
10. Cloud and SO_2 over ocean, $BT_{8.7} + BT_{10.8} - 2BT_{12.0} < \Delta BT_5$, where $\Delta BT_5 = -5.0$ K.
11. Test for water vapour and high altitude SO_2, $BT_{7.3} - BT_{6.2} > \Delta BT_6$, where $\Delta BT_6 = 20.0$ K.

Test 1 identifies potential ash pixels. The remaining test identifies possible false positives. Only the land emissivity test requires any model calculations. Real-time and archived results from this method and the VOLE-product from EUMETSAT are available from http://fred.nilu.no/sat/.

3.6 Neural networks

Researchers at the Ludwig-Maximilians University, Munich, and Deutsches Zentrum für Luft- und Raumfahrt, Oberpfaffenhofen, are developing a combined volcanic ash cloud detection and retrieval method based on neural networks. This is work in progress and nothing has been published about the method at the time of writing of this report.

3.7 Principal components analysis (Hillger and Clark, 2002)

Currently no principal components analysis (PCA) of SEVIRI images for volcanic ash cloud detection has been published. Hillger and Clark (2002) have used PCA to analysis Moderate Resolution Imaging Spectroradiometer (MODIS) images for ash situations. While an ash signal is clearly seen in the analysis, it is unclear how such a scheme may be used in an automated operational setting. The methodology, however, has potential and is thus mentioned here.

4 Comparison of Volcanic ash cloud detection methods

The various volcanic ash detection methods described in section 3, differ in their use of measured and modelled data and in the complexity of the various tests. The VOLE and KNMI methods may be said to be the simplest to implement as they rely on SEVIRI data only. The methods of Francis et al. (2012) and Pavolonis et al. (2013) utilizes radiative transfer models which require additional input data from for example weather forecast models and databases of surface emissivity. To have radiative transfer models running with input from weather forecast and combing the output with SEVIRI measurements requires careful implementation in an operational setting. Common to all methods are that they use thresholds based on specific eruptions. Thus, for future eruptions these thresholds may need re-tuning.

To quantitatively compare the various methods is challenging. They may be compared using both measured and modelled data. Surely, measured data are the acid test for any method. However, for measured data it is difficult to know which pixels are truly affected by ash, as no independent measurements are available for the full satellite image. Hence, here we use modelled SEVIRI scenes for the Eyjafallajökull 2010 eruption. For the simulated SEVIRI images the input ash fields are from the Flexpart dispersion model simulation (Stohl et al., 2011), hence it is also known which pixels that are affected by volcanic ash. Metorological clouds are included using data fra ECMWF. Further details about the simulated data set is given in Appendix B.

For each scene (time step) SEVIRI brightness temperature images are simulated for the 8.7, 10.8 and 12.0 μm channels. Examples of a simulated scene is shown in the left column of Fig. 2. The corresponding measured scene is shown in the right column. There are differences between the simulated and the measured brightness temperatures. Reasons for the differences are discussed by Kylling et al. (2013) and include coarser temporal and spatial resolution in the simulated data. The general large scale features are reproduced by the the model, including the ash signal seen starting from the south tip of Iceland and protruding southwards.

The VOLE-type (Prata and Prata, 2012), KNMI (de LaaT and van der A De Bilt, 2012), and Francis et al. (2012) ash detection methods have been used to extract ash information from the simulated scenes. An example with the VOLE-method detected ash is shown in Fig. 3. The upper plot shows the Flexpart ash column where only pixels with column density above 0.2 g/m^2 are included. The limit of 0.2 g/m^2 was chosen as this corresponds to the low contamination limit of 0.2 mg/m^3 for an ash cloud of 1 km vertical thickness defined in connection with the Eyjafjallajökull eruption (International Air Carrier Association (IACA), 2010). For 0600 UTC, 8 May, 2010, the Flexpart columns with ash columns above this limit are given as the union of blue and green pixels in the bottom plot of Fig. 3. The green colored pixels identify the pixels that are detected as ash from the simulated images using the ash VOLE-type detection method described above and whose Flexpart column is above 0.2 g/m^2. They represent coincident ash pixels from Flexpart and the simulated image/detection framework. The blue colored pixels are pixels that are identified as ash from the Flexpart simulations, but that fails detection by the simulated image/detection framework. They are thus false negatives. The red pixels are identified as ash by the simulated image/detection framework, but they should contain no ash according to the Flexpart simulations. They are false

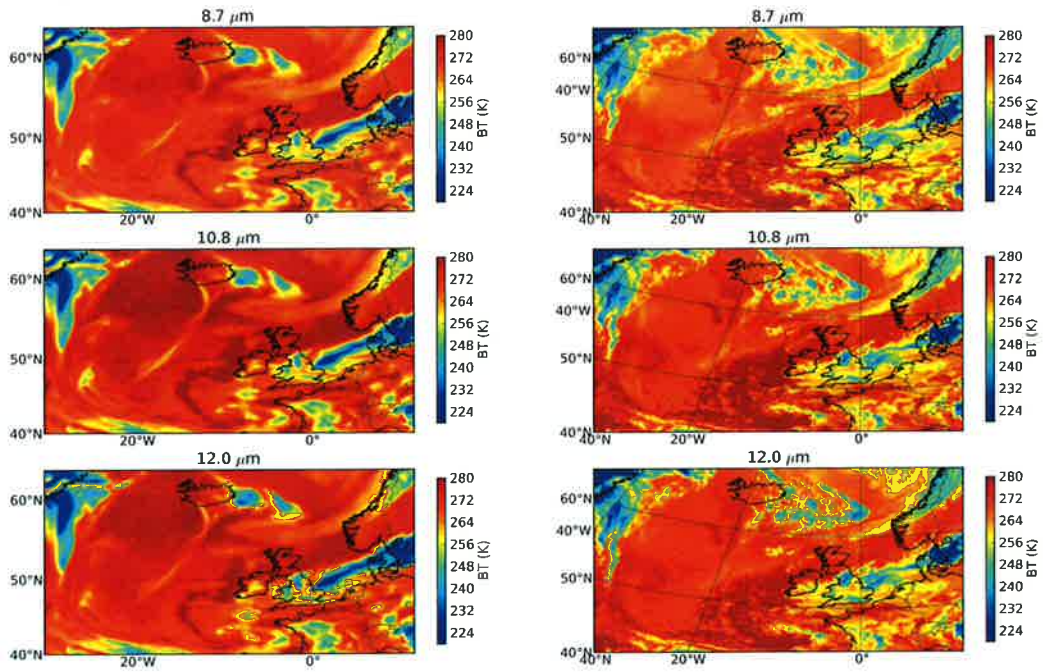

Figure 2: (Left column) The simulated brightness temperatures for the 8.7, 10.8 and 12.0 μm SEVIRI channels. (Right column) The brightness temperatures measured by SEVIRI for 8.7, 10.8 and 12.0 μm. All data for 0600 UTC, 8 May, 2010.

positives.

As an example the VOLE-type (Prata and Prata, 2012), KNMI (de LaaT and van der A De Bilt, 2012), and Francis et al. (2012) ash detection methods are compared in Fig. 4 for 0600 UTC, 8 May, 2010. Such comparisons were made for all simulated scenes (covering the period 14 April to 17 May 2010) and the number of coincidences, false negatives and false positives were calculated. The fraction of coincidences and false positives as a function of time are shown in Fig. 5. As can be seen from both the single case in Fig. 4 and from the time series in Fig. 5, all methods fail to detect all pixels with ash content above 0.2 g/m^2. The VOLE-method detects by far the most ash affected pixels and the KNMI-method the least. This is no surprise as the KNMI-method has more restrictive cut-off limits than the VOLE-method. This is also reflected in the number of false positives. The KNMI-method was designed to have few false positives which is evident from the red dashed line in Fig. 5. Both the VOLE- and Francis et al. (2012)-methods have far more false positives.

5 Conclusions

The nature of the problem and the information available from SEVIRI makes it impossible to detect all pixels possibly affected by ash. Here various ash detection methods have been compared quantitatively using realistic simulations of SEVIRI images for the Eyjafallajökull 2010 eruption.

Both the VOLE and KNMI ash detection methods rely on measured data only. They are thus easy to implement and operate on a routine basis. The β-ratio methods involves radiative transfer simulations that need input from weather forecast models or climatological data sets. As such they are both more complex to implement and demanding to run in an operational setting. They are also far more computer intensive, albeit still well within the requirements for an operational product.

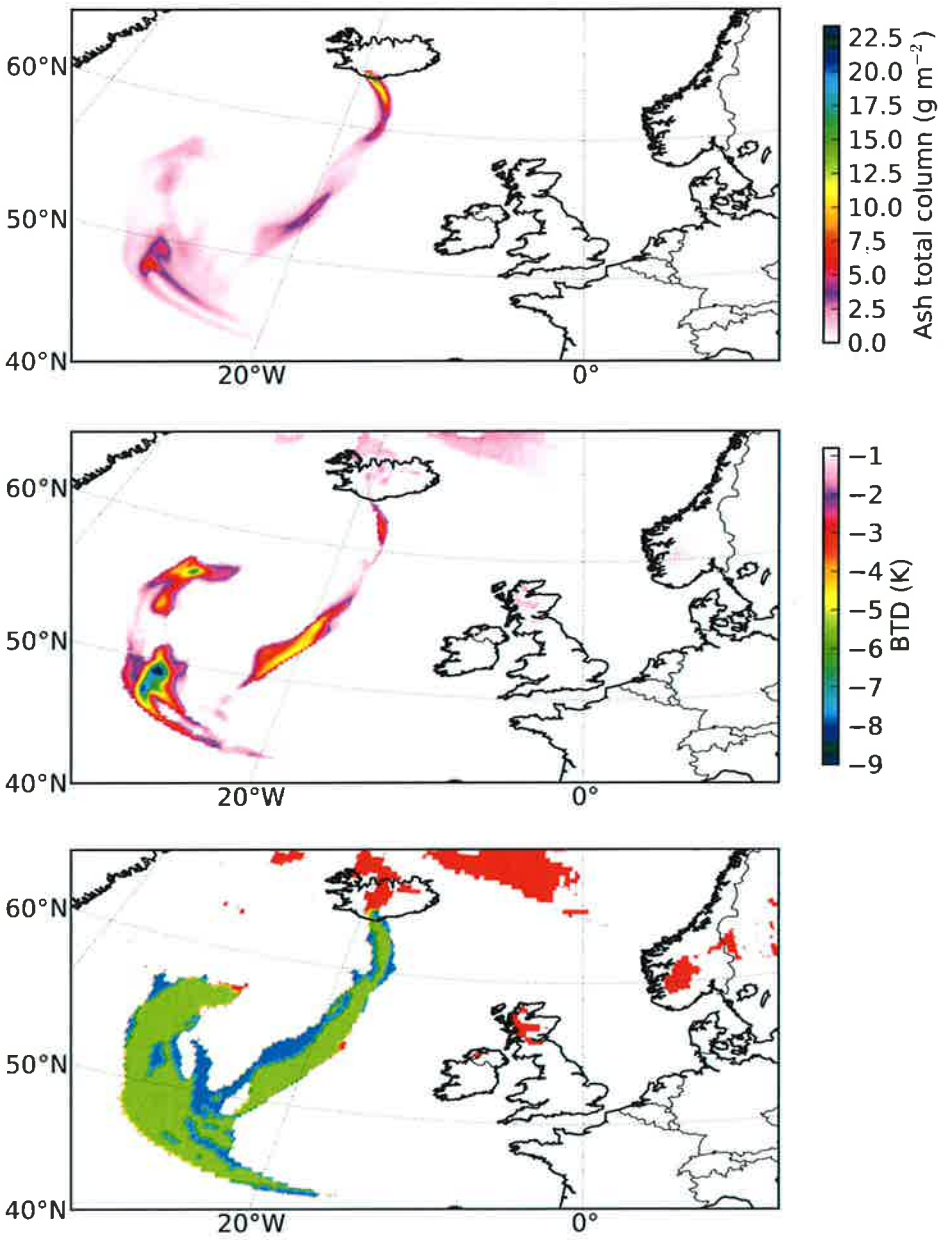

Figure 3: (Upper plot) The total ash column from the Flexpart model. (Middle plot) The brightness temperature difference $BT_{10.8} - BT_{12.0}$ from the MYSTIC simulations. (Bottom plot) Pixels identified as ash both from Flexpart and by the VOLE ash detection method (green, coincidences), pixels identified as ash only from Flexpart simulations (blue, false negatives, threshold 0.2 g/m^2) and pixels identified as ash from ash detection method only (red, false positives). All data are for 0600 UTC, 8 May, 2010.

In an operational setting one wants to avoid too many false positives. At the same time one wants to detect all pixels containing ash. The KNMI (de LaaT and van der A De Bilt, 2012) is robust and simple to implement, with

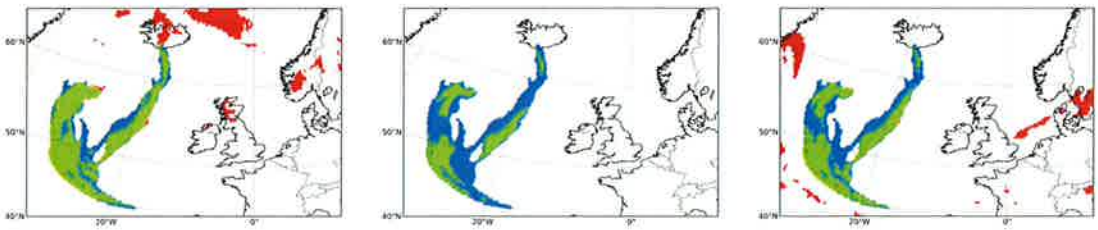

Figure 4: Comparison of the VOLE (left), KNMI (middle) and Francis et al. (2012) ash detection methods for 0600 UTC, 8 May, 2010. Pixels identified as ash both from Flexpart and by ash detection method (green, coincidences), pixels identified as ash only from Flexpart simulations (blue, false negatives, threshold 0.2 g/m^2) and pixels identified as ash from ash detection method only (red, false positives).

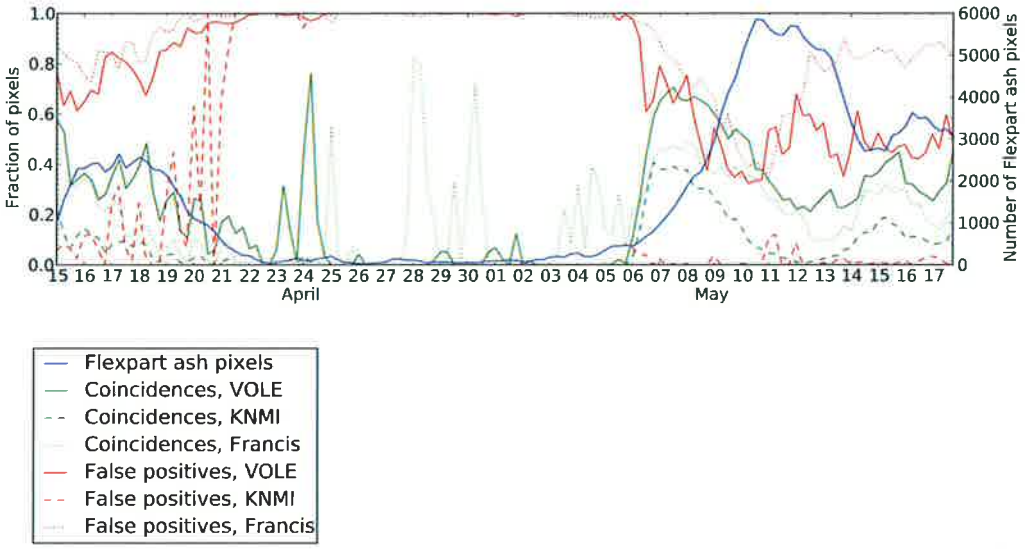

Figure 5: The number of Flexpart ash pixels (solid blue line, right hand axis) with column density larger than 0.2 g/m^2 as a function of time. Green lines show the fraction of coincidences between various ash detection methods and Flexpart ash pixels. The red lines gives the fraction of false positives. See text for further information.

few false positives, but may miss too many ash affected pixels. The VOLE-type (Prata and Prata, 2012) and Francis et al. (2012) ash detection methods detect more ash, but also have more false positives.

The methods investigated have different strenghts and weaknesses. As such it might be useful to run several detection methods and for example combine the VOLE-method with Francis et al. (2012): pixels where both methods find ash are identified as ash while pixels where only one method finds ash are classified as not being ash.

Finally, the VAST CID method may prove to be a powerful ash detection method. Due to the limitations in the present simulations framework this method could not be included in the present comparison. However, comparison between the VOLE product and the VAST CID is provided at `http://fred.nilu.no/sat/`.

References

Bohren, C. F. and Clothiaux, E. E.: Fundamentals of Atmospheric Radiation, Veimheim, Wiley-VCH, 2006.

Buras, R. and Mayer, B.: Efficient unbiased variance reduction techniques for Monte Carlo simulations of radiative transfer in cloudy atmospheres: The solution, J. Quant. Spectrosc. Radiat. Transfer, 112, 434–447, doi:10.1016/j.jqsrt.2010.10.005, 2011.

de LaaT, A. and van der A De Bilt, R.: Validation and evaluation of SEVIRI volcanic ash heights, Tech. rep., KNMI, TR-337, 2012.

Emde, C., Buras, R., Mayer, B., and Blumthaler, M.: The impact of aerosols on polarized sky radiance: model development, validation, and applications, Atmos. Chem. Phys., 10, 383–396, 2010.

Francis, P. N., Cooke, M. C., and Saunders, R. W.: Retrieval of physical properties of volcanic ash using Meteosat: A case study from the 2010 Eyjafjallajökull eruption, J. Geophys. Res., 117, doi:10.1029/2011JD016788, 2012.

Hillger, D. W. and Clark, J. D.: Principal component image analysis of MODIS for volcanic ash. Part I: Most important bands and implications for future GOES imagers, J. App. Met., 41, 985–1001, 2002.

International Air Carrier Association (IACA): Volcanic Ash - flying into areas of known or forecasted volcanic ash contamination, URL http://www.iaca.be/php/issues/index.php?doc_id=3688, 2010.

Kylling, A., Buras, R., Eckhardt, S., Emde, C., Mayer, B., and Stohl, A.: Simulation of SEVIRI infrared channels: a case study from the Eyjafjallajökull April/May 2010 eruption, Atmos. Meas. Tech., 6, 649–660, doi:10.5194/amt-6-649-2013, 2013.

Mayer, B. and Kylling, A.: Technical note: the libRadtran software package for radiative transfer calculations-description and examples of use, Atmos. Chem. Phys., 5, 1855–1877, 2005.

Mayer, B., Hoch, S. W., and Whiteman, C. D.: Validating the MYSTIC threee-dimensional radiative transfer model with observations from the complex topography of Arizona's Meteor Crater, Atmos. Chem. Phys., 10, 8685–8696, 2010.

Pavolonis, M. J.: Advances in extracting cloud composition information from spaceborne infrared radiances - a robust alternative to brightness temperatures. Part I: Theory, J. Appl. Met. Clim., 49, 1992–2012, 2010.

Pavolonis, M. J., Heidinger, A. K., and Sieglaff, J.: Automated retrievals of volcanic ash and dust cloud properties from upwelling infrared measurements, J. Geophys. Res., 118, 1–23, doi:10.1002/jgrd.50173, 2013.

Prata, A. J.: Infrared radiative transfer calculations for volcanic ash clouds, Geophys. Res. Lett., 16, 1293–1296, 1989.

Prata, A. J. and Grant, I. F.: Retrieval of microphysical and morphological properties of volcanic ash plumes from satellite data: Application to Mt Ruapehu, New Zealand", Q. J. R. Meteorol. Soc., 127, 2153–2179, 2001.

Prata, A. J. and Prata, A. T.: Eyjafjallajökull volcanic ash concentrations determined using Spin Enhanced Visible and Infrared Imager measurements, J. Geophys. Res., 117, D00U23, doi:10.1029/2011JD016800, 2012.

Prata, F.: Detecting and Retrieving Volcanic Ash from SEVIRI Measurements Algorithm Theoretical Basis Document, URL http://vast.nilu.no/media/cms_page_media/5/VAST_ATBD_SEVIRI_%Ash_v1.0_NILU_1.pdf, 2013.

Prata, F., Bluth, G., Rose, B., and adn Andrew Tupper, D. S.: Comments on "Failures in detecting volcanic ash from a satellite-based technique", Remote Sens. Environ., 78, 341–346, 2001.

Stohl, A., Hittenberger, M., and Wotawa, G.: Validation of the Lagrangian particle dispersion model FLEXPART against large scale tracer experiment data, Atmos. Env., 32, 4245–4264, 1998.

Stohl, A., Forster, C., Frank, A., Seibert, P., and Wotawa, G.: Technical note: The Lagrangian particle dispersion model FLEXPART version 6.2, Atmos. Chem. Phys., 5, 2461–2474, 2005.

Stohl, A., Prata, A. J., Eckhardt, E., Clarisse, L., Durant, A., Henne, S., Kristiansen, N. I., Minikin, A., Schumann, U., Seibert, P., Stebel, K., Thomas, H. E., Thorsteinsson, T., Tørseth, K., and Weinzierl, B.: Determination of time- and height-resolved volcanic ash emissions and their use for quantitative ash dispersion modeling: the 2010 Eyjafjallajökull eruption, Atmos. Chem. Phys., 11, 4333–4351, 2011.

Thomas, H. E. and Watson, I. M.: Observations of volcanic emissions from space: current and future perspectives, Nord. Hydrol., 54, 323–354, doi:10.1007/s11069-009-9471-3, 2010.

Wen, S. and Rose, W. I.: Retrieval of sizes and total masses of particles in volcanic clouds using AVHRR bands 4 and 5, J. Geophys. Res., 99, 5421–5431, 1994.

Wielicki, B. A. and Welch, R. M.: Cumulus cloud properties derived using Landsat satellite data, J. of Climate and Appl. Meteor., 25, 261–276, 1986.

Yu, T., Rose, W. I., and Prata, A. J.: Atmospheric correction for satellite-based volcanic ash mapping and retrievals using "split window" IR data from GOES and AVHRR, J. Geophys. Res., 107, doi:10.1029/2001JD000706, 2002.

A Derivation of equation for brightness temperature difference

Infrared (IR) radiation recorded by a satellite instrument viewing the Earth, is emitted from the Earth's surface and the Earth's atmosphere. The upward irradiance,$F_{\uparrow}(0)$, at the satellite may be written as (Eq. 5.108 Bohren and Clothiaux, 2006)

$$F_{\uparrow}(0) = F_{\uparrow} \exp(-\tau_{tot}) + \int_0^{\tau_{tot}} \exp(-\tau) B[\mathrm{T}(\tau)], \tag{20}$$

where τ_{tot} is the total optical depth of the atmosphere and B the Planck function at temperature T. For a plane-parallel ash cloud at constant temperature T_c and optical depth $\tau_{tot} = \tau_c$ (ignoring emission from other atmospheric constituents) Eq. 20 becomes

$$F_{\uparrow}(0) = B[\mathrm{T}_s] \exp(-\tau_c) + B[\mathrm{T}_c](1 - \exp(-\tau_c)). \tag{21}$$

Here the Earth's surface is assumed to be homogeneous with temperature T_s. Identifying the emissivity of the cloud, $\epsilon_i = 1 - \exp(-\tau_c)$, and the transmissivity, $t = \exp(-\tau_c)$ $(t + \epsilon = 1)$, Eq. 21 may be written in terms of brightness temperature, T, as (Prata and Grant, 2001):

$$T_i = \epsilon_i T_c + (1 - \epsilon_i) T_s. \tag{22}$$

If multiple scattering is ignored the emissivity may be written as (see for example eq. 2.24 Bohren and Clothiaux (2006))

$$\epsilon_i = 1 - \exp(-k_i L), \tag{23}$$

where L is the geometric thickness of the cloud and k_i is the absorption coefficient.

For SEVIRI observations at bands centered around 11 and 12 μm we get:

$$T_{11} = \epsilon_{11} T_c + (1 - \epsilon_{11}) T_s, \tag{24}$$

$$T_{12} = \epsilon_{12} T_c + (1 - \epsilon_{12}) T_s. \tag{25}$$

The brightness temperature difference $\Delta T = T_{11} - T_{12}$ thus becomes

$$\Delta T = (\epsilon_{12} - \epsilon_{11})(T_s - T_c). \tag{26}$$

From Eq.23 we have:

$$(1 - \epsilon_{11})^{k_{12}} = (1 - \epsilon_{12})^{k_{11}}, \tag{27}$$

or

$$\epsilon_{12} = 1 - (1 - \epsilon_{11})^{\beta} \tag{28}$$

where $\beta = k_{12}/k_{11}$. Inserting Eq. 28 in Eq. 26, solving Eq. 24 for ϵ_{11} and inserting in Eq. 26 gives (Eq. 5, Prata and Grant (2001)):

$$\Delta T = \Delta T_c (X - X^{\beta}). \tag{29}$$

where $\Delta T_c = T_s - T_c$, $X = 1 - \Delta_{11}/\Delta T_c$, and $\Delta_{11} = T_s - T_{11}$.

B Simulation of SEVIRI images

The simulation of SEVIRI images using Flexpart ash cloud fields, ECMWF ice and liquid water clouds as input to the MYSTIC radiative transfer model, has been described in detail by Kylling et al. (2013) and will only be briefly summarized here.

Stohl et al. (2011) used the Lagrangian particle dispersion Flexpart model (Stohl et al., 1998, 2005) to calculate the dispersion of ash from the Eyjafallajökull 2010 eruption. The ash concentration was calculated with a horizontal resolution of $0.25° \times 0.25°$ and a vertical resolution of 250 m for 25 particle size classes with radii in the range 0.125-125μm (see Stohl et al. (2011) for details). An example of the total ash column from the Flexpart model is given in the upper panel of Fig. 3. The ice and liquid water clouds were taken from European Centre for Medium-Range Weather Forecast (ECMWF) analysis. The horizontal resolution is $0.25° \times 0.25°$ and in the vertical data are provided at 91 model levels. The ECMWF data were interpolated to the Flexpart resolution as described by Kylling et al. (2013). ECMWF data are available every six hour. Thus, radiative transfer simulations were performed for 0, 6, 12 and 18 hours each day of the eruption (14 April-17 May). The radiative transfer calculations were made by the MYSTIC 3-D models (Mayer et al., 2010; Emde et al., 2010; Buras and Mayer, 2011) which was run within the libRadtran model framework (Mayer and Kylling, 2005). The MYSTIC model calculated brightness temperatures corresponding to the 10.8 and 12.0 μm channels and the geometry of the Spinning Enhanced Visible and Infrared Imager (SEVIRI) on board the Meteosat Second Generation (MSG, Meteosat-9) geostationary satellite. Images with ash and ice and liquid water clouds were calculated in addition to images containing only ash. A total of 135 images were calculated for each channel.

NILU – Norwegian Institute for Air Research
P.O. Box 100, N-2027 Kjeller, Norway
Associated with CIENS and the Fram Centre
ISO certified according to NS-EN ISO 9001/ISO 14001

REPORT SERIES SCIENTIFIC REPORT	REPORT NO. OR 39/2013	ISBN: 978-82-425-2651-9 (print) 978-82-425-2652-6 (electronic) ISSN: 0807-7207	
DATE 06/02/2014	SIGN.	NO. OF PAGES 16	PRICE NOK 150.-

TITLE	PROJECT LEADER
Measurement of volcanic ash in Norwegian air space WP 1.4.2 Improved detection of ash clouds	Nina I. Kristiansen NILU PROJECT NO. O-112109
AUTHOR(S) Arve Kylling	CLASSIFICATION * A CONTRACT REF.

QUALITY CONTROLLER: Nina I. Kristiansen

REPORT PREPARED FOR
Ministry of Transport and Communications and AVINOR

ABSTRACT
Water and ice clouds and temperature conditions may often influence the detection of volcanic ash affected pixels in infrared satellite images. Several methods are available for the detection of ash clouds in SEVIRI-images. Manual adjustments to the methods are often needed for a given ash situation.
The report describes various methods for detection of ash affected pixels. A quantitative comparison of the methods is made based on synthetic SEVIRI images from the 2010 Eyjafjallajokull eruption.

NORWEGIAN TITLE

Målinger av vulkanaske i norsk luftrom. WP 1.1.2 Forbedret deteksjon av askeskyer

KEYWORDS		
Volcanic ash	Remote sensing	Radiative transfer

ABSTRACT (in Norwegian)
Identifisering av aske i infrarøde satellittbilder forstyrres ofte av is- og vannskyer, samt de gitte temperatur forhold. Flere alternative metoder eksisterer for identifisering av askeskyer i SEVIRI-bilder. I en aktuell situasjon er ofte manuelle tilpasninger av deteksjonmetodene nødvendig.
Rapporten beskriver forskjellige metoder for identifisering av askeskyer. Metodene sammenlignes kvantitativt basert på syntetiske SEVIRI bilder for Eyjafjallajokull utbruddet i 2010.

** Classification*
A Unclassified (can be ordered from NILU)
B Restricted distribution
C Classified (not to be distributed)

REFERENCE: O-112109
DATE: JANUARY 2014
ISBN: 978-82-425-2651-9 (print)
978-82-425-2652-6 (electronic)

NILU – Norwegian Institute for Air Research is an independent, nonprofit institution established in 1969. Through its research NILU increases the understanding of climate change, of the composition of the atmosphere, of air quality and of hazardous substances. Based on its research, NILU markets integrated services and products within analyzing, monitoring and consulting. NILU is concerned with increasing public awareness about climate change and environmental pollution.